JTTEE5 7:489-496

PEER REVIEWED

X-ray Residual Stress Measurement in Metallic and Ceramic Plasma Sprayed Coatings

J. Matejícek, S. Sampath, and J. Dubsky

(Submitted 14 June 1997; in revised form 18 May 1998)

Processing-induced residual stresses play an important role in the production and performance of thermally sprayed coatings. Their precise determination is a key to influence the coating properties by modification of process variables and to understand the processing-structure-property relationship. Among various methods for residual stress measurement, x-ray diffraction holds a specific position as being nondestructive, phase distinctive, localized, and applicable for real parts. The $\sin^2 \psi$ method is commonly applied for bulk materials as well as coatings. However, the results are often reported without sufficient experimental details and the method is used in its simplified form without justification of certain assumptions.

In this investigation, the $\sin^2 \psi$ x-ray diffraction method was used to measure residual macrostress in plasma sprayed metallic (nickel, NiCrAlY, and molybdenum) and ceramic (ZrO_2 + 8%Y_2O_3) coatings. Reproducibility of the method was tested and the assumptions allowing its use are discussed and experimentally verified. For nickel coatings, a comparison with hole drilling and neutron diffraction measurements is presented. The influence of processing factors such as deposition temperature and coating thickness is studied and the results are discussed.

Keywords residual stress, x-ray

1. Introduction

Thermally sprayed nickel alloys and yttria-stabilized zirconia (YSZ) are among the most commonly used materials for thermal barrier and other high temperature coatings. The ceramic coating, due to its low thermal conductivity and thermal shock resistance, provides the desired insulation, whereas the metallic deposit serves as an intermediate bonding layer between the top coating and the substrate. Molybdenum finds applications in various wear-resistant and low-friction coatings. Large temperature differences experienced during thermal spray processing lead to residual stresses in the component, and they strongly affect its performance. In service, applied stress is superimposed on the residual stress and, depending on their respective sign, may either add up or reduce each other, with consequential effects on failure. Therefore, it is important to understand the stress state before the component enters the service and through better understanding of the stress development, modify the spraying process so that it leads to a favorable condition.

Residual stresses have two main origins:

- Rapid quenching of molten droplets upon impact on the substrate with restricted contraction. Such a large temperature drop (~ 2000 °C) would lead to stress that the material could not withstand; therefore, the resulting level is limited by the intrinsic strength of the splat and adhesion to the underlying substrate. The stress originating from splat quenching is always tensile.
- Cooling of the completed deposit and substrate couple from deposition to ambient temperature, when the stresses develop due to differences in thermal expansion. The so-called thermal mismatch stress can be compressive or tensile.

In addition, the stress levels are affected by a number of other factors, such as temperature gradients during and after deposition, stress relaxation processes (plastic deformation, cracking, intersplat sliding, self-annealing, etc.), phase transformations, chemistry changes, compliance of the substrate and coating, etc.

The complexity and simultaneous occurrence of these phenomena, together with limited knowledge of the properties of the constituent (which vary a great deal with processing parameters), hinders advancement of reliable models to predict the stress levels and emphasizes the importance of experimental methods. There are a number of approaches to stress determination, each of which has certain advantages, drawbacks, and limitations (Ref 1).

The most popular methods of residual stress measurement in coatings can be roughly divided into three groups: material removal methods, substrate curvature measurement, and diffraction methods.

Material removal methods are based on measurement of small dimensional changes associated with removal of the stressed part of the specimen, either by drilling a hole in the coating/substrate (Ref 2) or by grinding off a coating layer (Ref 3). The strain changes are monitored with strain gauges attached to the coating or the substrate, respectively. These methods have a significant advantage in capability to determine through-thickness stress gradients. Also, similar principles could be used to evaluate the mechanical properties of the coating (Ref 4). However, there are two major problems with the use of these methods: risk of damage to the coating and stress alteration (Ref 5) and difficulty to control a uniform material removal. Further limitations are imposed by the necessity of knowing the

J. Matejícek and **S. Sampath,** Center for Thermal Spray Research, State University of New York, Stony Brook, NY 11794-2275; and **J. Dubsky,** Institute of Plasma Physics, Za Slovankou 3, 182 11 Praha 8, Czech Republic.

mechanical properties of the constituents and by dimensional requirements.

Another very common method of stress determination is based on optical or mechanical measurement of substrate curvature, induced by stress in the coating (Ref 6-8). This method, in its simplest form, can determine only average stress value in the coating, and has severe limitations on specimen shape and dimensions. More information about stress distribution can be obtained if dimensional changes of both the coating and the substrate are measured after detachment (Ref 9). The analysis becomes quite complex if thicker coatings or multilayers are studied, and especially if plastic deformation of the substrate occurs. Among the most important advantages of this approach are relatively simple experimental setup, direct determination of coating stress (most of the other methods measure strain), ability to observe stress changes in situ during deposition (Ref 10), and separation of the contributions of quenching and thermal mismatch stresses (Ref 11).

This article deals with x-ray diffraction (XRD), whose characteristics are:

- It is nondestructive; therefore, the same specimens can be used for other investigations, or repeated measurements can be performed on specimens undergoing various treatments, fatigue, and so forth (Ref 12).
- It is phase distinctive, that is, capable of stress determination in each phase.
- It has moderate restrictions on specimen dimensions and shape; therefore, it can be used for measurements on various specimen sizes and components.
- Due to the low penetration of x-rays, the investigated volume is limited to a thin surface layer (in order of tens of μm), comprising of few splat thicknesses. This feature represents certain advantages and limitations at the same time.

In the following section, the principle of macrostress determination by XRD is briefly outlined. The experimental technique used is described, including characteristics of the specimens and measurement conditions. The results are then presented and discussed in light of certain assumptions allowing a simplified form of general formulas to be used. Finally, the role of material and processing characteristics is discussed, particularly the effect of deposition temperature and coating thickness on residual stress.

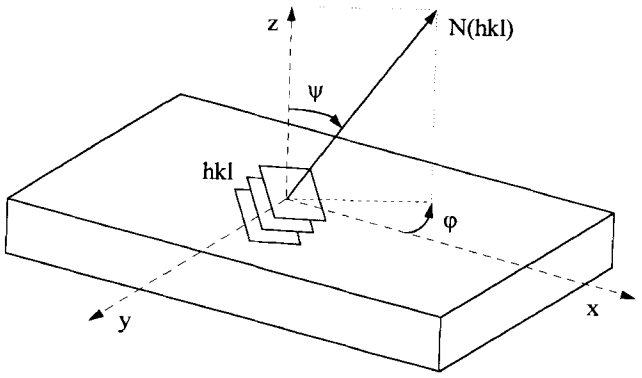

Fig. 1 Schematic of specimen and measurement coordinates. *x*, *y*, and *z* axes in the specimen coordinate system; *hkl*, Miller's indices of the diffracting crystal planes; *N*(*hkl*), normal to these planes (scattering vector, direction of measured strain); φ and ψ, angles defining the *N*(*hkl*) direction with respect to axes *x*, *y*, and *z*

2. XRD Stress Measurement Method

The diffraction method of stress determination is based on the measurement of changes in crystal plane spacing in different directions with respect to the specimen surface, which exhibit themselves as shifts in angular positions of respective diffraction peaks. From this strain determination, stress can be calculated with the use of appropriate elastic constants.

The crystal plane spacing in a given direction is determined from the peak position using Bragg's law:

$$n\lambda = 2d\sin\theta \qquad \text{(Eq 1)}$$

where n is the reflection order (usually only the first order is encountered for most common crystal structures), λ is the radiation wavelength, d is the plane spacing, and θ is the diffraction angle. The strain is then given by:

$$\varepsilon = (d - d_0)/d_0 \qquad \text{(Eq 2)}$$

where ε is the strain in a particular direction, d is the stressed, and d_0 the unstressed interplanar spacing. The general relationship between strain and stress is as follows (Ref 13):

$$\varepsilon_{ij} = \tfrac{1}{2} S_2 \sigma_{ij} + \delta_{ij} S_1(\sigma_{XX} + \sigma_{YY} + \sigma_{ZZ}) \qquad \text{(Eq 3)}$$

ε_{ij} being components of the elastic strain tensor, σ_{ij} components of the stress tensor in the specimen coordinate system (in this article, x and y axes are parallel to the specimen length and width in the coating plane, and the z axis is perpendicular to the coating plane, see Fig. 1), $\delta_{ij} = 1$ for $i = j$, $\delta_{ij} = 0$ for $i \neq j$, and $\frac{1}{2}S_2$, and S_1 are crystallographic elastic constants. For isotropic materials, they are related to Young's modulus and Poisson's ratio through the following relationship:

$$\tfrac{1}{2} S_2 = (1 + \nu)/E \qquad \text{(Eq 4)}$$

and

$$S_1 = -\nu/E \qquad \text{(Eq 5)}$$

For anisotropic materials, they can be either calculated from single-crystal elastic constants S_{ij} or determined experimentally. The strain in a given direction is then related to principal stresses as:

$$\begin{aligned}\varepsilon = {} & \tfrac{1}{2} S_2[(\sigma_{XX}\cos^2\varphi + \sigma_{XY}\sin 2\varphi + \sigma_{YY}\sin^2\varphi - \sigma_{ZZ}) \\ & \sin^2\psi + \sigma_{ZZ}] \\ & + \tfrac{1}{2} S_2 (\sigma_{XZ}\cos\varphi + \sigma_{YZ}\sin\varphi)\sin 2\psi \\ & + S_1 (\sigma_{XX} + \sigma_{YY} + \sigma_{ZZ})\end{aligned} \qquad \text{(Eq 6)}$$

where the angles ψ and φ denote the measurement direction; ψ is the angle between the sample surface normal and crystal plane normal, and φ is the azimuthal angle in the surface plane (Fig. 1).

The commonly used "$\sin^2\psi$" method uses a simplified form of this formula:

$$\varepsilon = \tfrac{1}{2} S_2 \sigma_\varphi \sin^2 \psi + S_1 (\sigma_{XX} + \sigma_{YY}) \quad \text{(Eq 7)}$$

with

$$\sigma_\varphi = \sigma_{XX} \cos^2 \varphi + \sigma_{XY} \sin 2\varphi + \sigma_{YY} \sin^2 \varphi \quad \text{(Eq 8)}$$

which applies under the following conditions (Ref 13):

- The stress is constant within the investigated volume; that is, there are no significant gradients, and σ_{ZZ} (stress perpendicular to the surface plane) equals 0 within the penetration depth.
- Two of the stress principal axes are parallel to the surface plane.
- The material has a random distribution of crystal orientations (no texture).

The applicability of this approach is examined in this article.

3. Experimental Details

Materials and Specimens. Table 1 summarizes some of the relevant specimen characteristics. For each of the NiCrAlY and YSZ coatings, a set of five specimens on 50 by 25 by 2.5 mm steel substrates was used for reproducibility assessment and one specimen on 120 by 25 by 2.5 mm substrate was used for comparison of applied and measured strain in three-point bending. For nickel and K20 coatings, one specimen of each type, as described in Table 1, was examined. For the study of deposition temperature effects, molybdenum coatings were deposited on 50 by 25 by 2.5 mm steel substrates and 50 by 25 by 3.3 mm aluminum substrates at three different temperatures: 190, 260, and 440 °C. Different temperatures were achieved by varying the amount of substrate preheating and air cooling during deposition. For the thickness effect study, six molybdenum specimens were prepared on 0.7 mm steel substrates, with thickness varying from 0.1 to 0.9 mm. These were all deposited at the same time. Different thicknesses were achieved by removing one specimen at a time from the chamber when a given thickness was reached, while the deposition of the remaining specimens continued until the final thickness.

The YSZ coating consisted primarily of tetragonal t' phase, with about 1% monoclinic phase. Cubic phase, if present, was not distinguished from the t' phase. Nickel, NiCrAlY, and molybdenum coatings were 100% cubic phase.

Measurements. Macrostress and phase analysis measurements were performed on Siemens D500 ω-diffractometer (Siemens AG, Karlsruhe, Germany) with nickel-filtered copper radiation ($\lambda = 0.15405$ nm). For nickel and nickel alloy coatings, the (331) and (420) reflections were used, with 2θ positions of ~145 and ~156°. For YSZ coatings, the (206) and (620) reflections at ~142 and ~144° were used. For molybdenum coatings, the (321) reflection at ~133° was used. The peak position was determined at 10 different ψ tilts (2×0, ±15, ±30, ±45, ±60), from at least 75 points forming the peak profile. The strain values were then converted to stresses using bulk elastic constants $E = 217$ GPa and $\nu = 0.29$ for nickel and nickel alloys, $E = 200$ GPa, and $\nu = 0.3$ for YSZ, and $E = 300$ GPa and $\nu = 0.29$ for molybdenum. Microstrain measurements were performed on a Philips PW1729 diffractometer (Philips Analytical X-Ray, Mahwah, NJ) with nickel-filtered copper radiation on a set of at least five distinct reflections. Microstrain values were calculated from the dependence of peak width on diffraction angle according to Ref 14. For comparison of applied and measured strain, a simple three-point bending device was mounted in the diffractometer, and the loading element displacement was measured with a dial gauge.

4. Results and Discussion

4.1 Examination of the Method

Instrumental Effects. The instrumental effects must be separated from the physical phenomena observed. One important phenomenon occurring during this kind of measurement is the loss of focusing when $\psi \neq 0$, with a subsequent decrease in peak height and increase in width (Ref 15). This effect was minimized by using (*hkl*) reflections with high diffraction angle. In order to assess the influence of defocusing on peak position, measurements were performed on NiCrAlY starting powder and YSZ sprayed and water-quenched powder specimens at exactly the same conditions as the stress measurements on coatings. The

Table 1 Specimen characteristics

Material	Composition, wt%	Powder	Process	Coating thickness, mm	Substrate dimensions, mm	State of the coating
NiCrAlY	Ni + 16.5Cr + 5.5Al + 0.5Y	Praxair Ni-346-1	APS	0.2	50 × 25 × 2.5	As-sprayed
NiCrAlY	Ni + 16.5Cr + 5.5Al + 0.5Y	Praxair Ni-346-1	APS	0.2	120 × 25 × 2.5	As-sprayed
YSZ	ZrO2 + 8Y2O3	H.C. Starck 825.1	APS	0.2	50 × 25 × 2.5	As-sprayed
YSZ	ZrO2 + 8Y2O3	H.C. Starck 825.1	APS	0.2	120 × 25 × 2.5	As-sprayed
Ni	Ni	Amdry 917	APS	0.1	50 × 15 × 2.5	As-sprayed
Ni	Ni	Amdry 917	VPS	0.6	25 × 25 × 2.5	Ground
Ni	Ni	Amdry 917	VPS	0.6	25 × 20 × 2.5	Polished
K20	Ni + 2.5Si + 1.5B	Metalurgicke zavody K20	WSP	1.0	28 × 17 × 2.5	As-sprayed
K20	Ni + 2.5Si + 1.5B	Metalurgicke zavody K20	WSP	1.0	28 × 17 × 2.5	Ground
Mo	Mo	Osram Sylvania Mo SD152	APS	0.003	50 × 25 × 2.5	As-sprayed
Mo	Mo	Osram Sylvania Mo SD152	APS	Varying	50 × 20 × 0.7	As-sprayed
Steel	Fe + 13Cr + 1Mn + 1Si	SVUM AISI 410	HVOF	0.68	120 × 25 × 2.5	As-sprayed

APS, atmospheric plasma spraying; VPS, vacuum plasma spraying; WSP, water-stabilized plasma (ambient atmosphere); HVOF, high-velocity oxygen fuel

results, 13 ± 3 MPa for NiCrAlY and −11 ± 10 MPa for YSZ, served as the instrument calibration. All other "artificial" effects pertinent to this individual instrument (Ref 16) were taken into account by this procedure.

Reproducibility. The reproducibility of the stress measurements and of the spraying procedure were checked on sets of five specimens for NiCrAlY and YSZ coatings. For some specimens, measurements were repeated by another experimenter as well. Table 2 summarizes resulting values of in-plane stress in the direction parallel to the specimen length. It can be seen that the results are consistent within the experimental error. Standard deviations of stress values are approximately 15 MPa, which is comparable in accuracy to routine measurements on bulk materials.

Texture and Anisotropy. Texture is an important feature of many coatings. Because the term "texture" is commonly assigned to three different phenomena, they are briefly reviewed here for distinction:

- Preferred orientation (crystallographic texture): Nonrandom distribution of crystal orientations with respect to the specimen. It manifests itself by intensity variation of a particular (*hkl*) reflection in different directions. This phenomenon frequently occurs in coatings, especially those produced by chemical vapor deposition (CVD) and physical vapor deposition (PVD) techniques. In the case of plasma spraying, rapid cooling can result in preferred growth of certain crystal planes in the heat flow direction (Ref 17).
- Shape of crystal grains: Columnar grain structure inside the splats is typical for plasma sprayed coatings, with the columns growing mostly perpendicular to the coating plane. In addition, ultrafine structures were observed in certain cases (Ref 18).
- Lamellar structure of the coating: Consists of thin, elongated splats and voids of various shapes and orientations (Ref 19, 20). This is a major factor contributing to the macroscopic anisotropy.

Table 2 Stress results from NiCrAlY and yttria-stabilized zirconia specimens

Specimen	σ_{XX}, MPa	σ_{XX}, corr
NiCrAlY		
1	115 ± 15	112 ± 19
1R	89 ± 12	87 ± 12
2	80 ± 16	110 ± 18
3	100 ± 13	114 ± 14
4	108 ± 10	108 ± 10
5	85 ± 11	105 ± 14
Average	**99 ± 15**	**104 ± 10**
Yttria-stabilized zirconia		
1	10 ± 12	...
2	20 ± 5	...
3	23 ± 11	...
4	−5 ± 8	...
5	23 ± 7	...
5R	23 ± 6	...
Average	**15 ± 10**	...

σ_{XX} is the stress in the coating plane. In the specimen labels, R denotes repeated measurement on the same specimen. The third column presents data corrected for plasticity-induced texture. (For details see text.)

For all the measurements in this study, intensity variation with the ψ angle was monitored for diffraction peaks used in stress measurement. No significant difference was observed between coatings and powder reference samples, which suggests that no strong crystallographic texture was present. Strong texture is more likely to develop only in a very thin layer close to the substrate, where the most rapid cooling takes place, and rather in high thermal conductivity materials (Ref 21, 22).

Nevertheless, a slight common variation in the intensity versus $\sin^2\psi$ plots were observed in NiCrAlY specimens. Similarity with d versus $\sin^2\psi$ suggested plastic interaction between the grains as a probable mechanism. These data were treated according to the procedure of Marion and Cohen (Ref 23) and are reported in the third column of Table 2. It can be seen that the data are not altered to a major extent, but their scatter is somewhat lower after this correction.

Elastic anisotropy, that is, dependence of stiffness on (*hkl*) direction in the crystal, was investigated on (331) and (420) reflections of nickel coatings (see Table 3). The stresses calculated using macroscopic values of E and ν agreed within experimental error. The average ratio of $\sigma_{XX}(420)$ and $\sigma_{XX}(331)$ was found to be 1.25, which is relatively close to the ratio of respective elastic constants (1.16) reported in (Ref 24). This indicates small relative anisotropy in these directions.

The effect of the macroscopic anisotropy of the coating was studied by Ceretti et al. (Ref 25). Elastic constants in three principal directions were determined by comparing applied and measured stresses in plasma sprayed steel coating. No significant differences between the values for different directions were observed.

Triaxial/Biaxial Stress. The validity of the biaxial stress assumption (i.e., $\sigma_{ZZ} = 0$ within the depth investigated by x-rays) was examined for all three types of coatings. First, the stress in the width direction, y, in the coating plane was measured for NiCrAlY and YSZ coatings. The values (93 ± 19 MPa for NiCrAlY, specimen 1, and 14 ± 8 MPa for YSZ, specimen 5) agreed with those in x-direction within experimental error. However, this may not apply for thick coatings of largely unequal x and y dimensions and for more complex shapes (e.g., cylinders). Therefore, measurement in both directions is recommended. Second, the stress in the z-direction (perpendicular to the coating plane) was determined from these two measurements, following the procedure described in Ref 24. The value was effectively zero for both coatings and was confirmed by a d_0 calculation from the $\sigma_{11} + \sigma_{22} = \sigma_{XX} + \sigma_{YY}$ equality ($\sigma_{11} + \sigma_{22}$ being the sum of principal stresses in the coating plane). This was expected, in view of the coating generation (contraction of the solidifying splats is restricted only in the direction parallel to

Table 3 Residual stresses in various nickel-base coatings, determined from (331) and (420) reflections (calculated using the same macroscopic elastic constants)

Specimen	$\sigma_{XX}^{(331)}$, MPa	$\sigma_{XX}^{(420)}$, MPa
Ni-APS	51 ± 12	74 ± 12
Ni-VPS-polished	−114 ± 7	−117 ± 7
Ni-VPS-ground	−161 ± 6	−205 ± 12
K20	23 ± 12	38 ± 6

APS, atmospheric plasma spraying; VPS, vacuum plasma spraying

the surface) and low penetration depth of x-rays. Nevertheless, nonzero values of σ_{ZZ} within the penetration depth can occur in multiphase materials.

Surface Effects. Because of the low penetration of x-rays (~16 μm in nickel, ~8 μm in YSZ), the surface state of the specimen can influence the results. For example, if the surface roughness is comparable to the penetration depth, stress relaxation on the asperities can contribute to lower measured values than would be observed under a smooth surface. Table 4 reports the surface roughness of the specimens under investigation. When comparing the roughness with the effective penetration depth, one can conclude that the values determined by x-rays may be slightly underestimated with respect to stress deeper below the surface. Conversely, surface modification techniques, like grinding and polishing, that decrease the roughness, can alter the stress state to a significant degree, as mentioned in the following paragraphs for nickel alloy coatings.

In the ground K20 coating, a significant ψ-splitting (difference between positive and negative ψ tilts) was observed, which makes the commonly used linear fit to ε versus $\sin^2 \psi$ data not applicable. This phenomenon is explained either by the presence of shear stresses with a nonzero component in the z-direction (Ref 26-28), dislocation density variations (Ref 29), inhomogeneous inclinations of crystal lattice planes as grains conform to their neighbors to prevent creation of voids (Ref 30) or by presence of stress couples (Ref 31). Some of these theories are alternative; some are rather complementary (Ref 31). Discussion of the origin of ψ-splitting lies beyond the scope of this article; suffice it to say that the surface stress state can be significantly altered by grinding, which makes this procedure unusable for surface roughness reduction when x-ray stress measurements are to be performed. The magnitude of this effect depends on various factors, for example, the loading force, speed, direction of motion, and roughness of the grinding media. The magnitudes of ψ-splitting in both ground and polished vacuum plasma spraying (VPS) nickel coatings were negligible, but no unmodified counterparts were available for comparison.

Stress Gradient. The difference in penetration of x-rays at different incidence angles allows assessment of stress gradient in the thickness direction (Ref 13, 32). If linear dependence of stress on depth is assumed:

$$\sigma_\varphi(T) = \sigma_{\varphi 0} + KT \quad \text{(Eq 7)}$$

($\sigma_{\varphi 0}$ is the surface stress, K the stress gradient, and T the penetration depth), then the average observed stress:

$$\langle \sigma_\varphi \rangle = \sigma_{\varphi 0} + K \cos \psi / \mu_0 \quad \text{(Eq 8)}$$

(μ_0 is the linear absorption coefficient) is substituted for σ_φ in Eq 6, and the measured strain data are fitted with a function comprising of three parameters ($\sigma_{\varphi 0}$, K, $\sigma_{XX} + \sigma_{YY}$) instead of two. This procedure could be generalized to any function describing the depth dependence of stress; for n new parameters, at least $n + 2$ strain measurements are necessary. Assuming linear dependence on the depth, gradient $\partial\sigma_{XX}/\partial z$ for VPS nickel coatings was determined to be -14 ± 3 MPa/μm (i.e., more compressive near the surface). Such a high gradient cannot be sustained throughout the entire coating thickness; it is probably contained only within the surface layer, due to the fact that it is attached only by one side to the rest of the body. Stress gradients in all of the other coatings were small compared to experimental error.

Correlation to Macroscopic Deformation. In order to correlate the deformation measured within individual crystal grains to the macroscopic deformation of the coating, series of measurements were taken during three-point bending of NiCrAlY and YSZ coatings. The measured strain versus applied strain dependence showed an initial increase, but after a relatively small strain (150×10^{-6} for NiCrAlY, and 40×10^{-6} for YSZ) exhibited random oscillations with no clear correlation to applied strain. After unloading, the measured strain remained approximately the same as at maximum load. In contrast to results of Tobe et al. (Ref 33), who used much higher applied strains, the macrostrain pattern was closely followed by microstrain, thus supporting the validity of the results. Low strength of the coatings and possibly loose bonding of the top layer of splats is thought to be responsible for this behavior. No macroscopic cracking was observed. The effective elastic constants calculated from the initial slope were 320 GPa for NiCrAlY and 78 GPa for YSZ, but these should be considered only very approximate, due to the low number of data available for calculation. Nevertheless, measurements during a four-point bending test on high-velocity oxygen fuel (HVOF) deposit of AISI 410 stainless steel showed smooth linear behavior and good agreement of measured stresses during loading and unloading stages. Young's modulus calculated from the measured versus applied strain curves was 58 GPa, slightly less than ⅓ of the value of corresponding bulk material, a value typically encountered in thermally sprayed deposits (Ref 34). Aside from the porous structure, this value may be affected by a relatively high amount of $(Fe,Cr)_3O_4$ oxides (Ref 35).

Comparison with Other Methods. Results of hole-drilling measurements of residual stress were available for the nickel coatings; in addition, measurements by neutron diffraction were performed. Table 5 summarizes the results. As can be seen, all three methods yielded qualitatively comparable results, although the magnitudes were different. It should be noted that the diffraction methods measure strain in coherently diffracting crystalline domains, whereas the "macroscopic" strain measured by hole drilling or deflection methods may encompass crack opening and intersplat sliding. This, together with possible surface roughness relaxation, can account for the lower stress value observed in atmospheric plasma sprayed (APS) coating using XRD, compared to the result of the hole-drilling method. The origin of higher XRD stress value in vacuum plasma sprayed (VPS) coating could be associated with the observed gradient. Neutron diffraction measures the same quantity as x-ray diffraction, but over a different volume, the

Table 4 Surface roughness of the specimens

Specimen	Surface roughness (R_a), μm
NiCrAlY	13.3
YSZ	7.3
Ni-VPS polished	1.0
Ni-VPS ground	2.0
Ni-APS	14.1

APS, atmospheric plasma spraying; VPS, vacuum plasma spraying

values reported in Table 5 are averages over the entire coating thickness. Further discussion of these results follows in the next section.

4.2 Material and Processing Factors

NiCrAlY and YSZ Coatings. The tensile stress present in the NiCrAlY coatings (Table 2) is thought to be a result of restrained contraction during splat quenching because the difference in thermal expansivity between the coating and the substrate is relatively small to account for significant thermal mismatch stress. The values are comparable in magnitude to those measured by Kuroda et al. (Ref 36) in Ni + 20Cr coatings and by Greving et al. (Ref 3) in Ni + 5Al coatings. The stress values in the YSZ specimens are close to zero. This seems to indicate that the ceramic coating is too brittle to contain a high stress and this relaxes by intersplat and intrasplat cracking. Metallographic observation also showed weak bonding to the substrate. Furthermore, in this case, the quenching stress and the thermal mismatch stress have opposite signs and may thus cancel each other under the spraying conditions used. In fact, both tensile and compressive stresses were observed in YSZ coatings, depending on the substrate temperature (Ref 37, 38).

Table 5 Residual stresses in atmospheric plasma sprayed and vacuum plasma sprayed nickel coatings, determined by various methods

Specimen method	Ni-APS, σ_{XX}, MPa	Ni-VPS, σ_{XX}, MPa
XRD	62	-116
HD	241	-55
ND	186	-37

APS, atmospheric plasma spraying; VPS, vacuum plasma spraying; XRD, x-ray diffraction; HD, hole drilling; ND, neutron diffraction

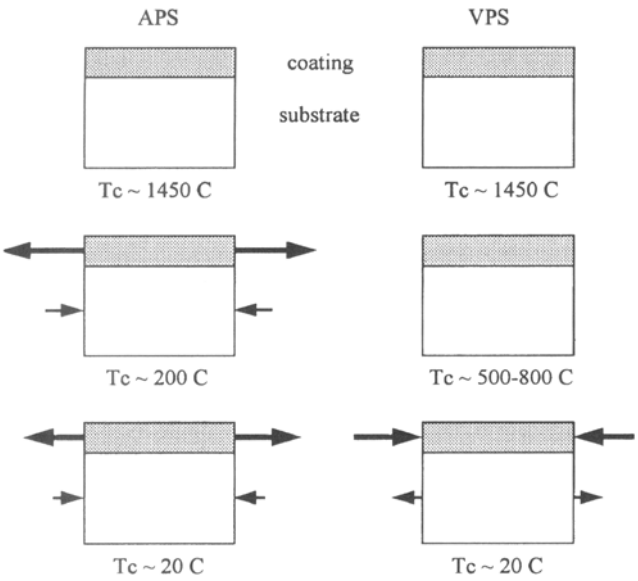

Fig. 2 Schematic of the stress development during various stages of coating deposition. (a) At impact (particle at melting temperature; both coating and substrate are stress free). (b) After solidification (both parts at deposition temperature; for atmospheric plasma spraying (APS), coating is under tension, substrate under small compression; for vacuum plasma spraying (VPS), stresses are reduced due to annealing at high deposition temperature). (c) After cooling to room temperature. (Thermal mismatch stress is added to previous stress; because coefficient of thermal expansion (CTE)(Ni) $\cong 13 \times 10^{-6}$/C and CTE(steel) $\cong 14 \times 10^{-6}$/C, this stage adds compression to the coating and tension to the substrate). T_C is coating temperature; outward arrows indicate tensile stress, and inward arrows indicate compressive stress.

Nickel Coatings. Table 3 shows results from nickel coatings processed by two distinct techniques: atmospheric and vacuum plasma spraying. The APS coating was found to be under tension, whereas the VPS coating was under compression. This can be explained by the higher deposition temperature in the case of VPS, which amplifies the contribution of thermal mismatch stress compared to the quenching stress. Because the coefficient of thermal expansion (CTE) of the coating is slightly smaller than the CTE of the substrate, the thermal mismatch stress is compressive in the coating. The quenching stress is always tensile, but its magnitude differs for both processes (see Fig. 2). For APS, quenching stress values in the order of 100 MPa can be retained in the coating (Ref 10), whereas in the case of VPS it diminishes due to self annealing at higher temperatures achieved during VPS processing. Evidence to this effect can be seen in Fig. 3, which shows a transmission electron micrograph of a lateral section of a VPS nickel coating. Dislocation cells are visible in the micrograph, indicating that recovery and polygonization (precursor to recrystallization) have occurred (Ref 39).

Molybdenum Coatings. Figure 4 shows the effect of deposition temperature on residual stress in thin molybdenum coatings (approximately one layer of splats) on steel and aluminum substrates. It can be seen that for both substrates the stresses change from tensile to compressive as the temperature rises. This can be explained by the different proportion of quenching and thermal stress, which have opposite signs. The quenching stress is tensile, whereas the thermal stress is in this case compressive because the thermal expansivity of molybdenum is smaller than that of steel and aluminum. When the deposition temperature is higher, the thermal stress upon cooling to room temperature is higher; therefore, the residual stress, being a sum of quenching and thermal stresses, shifts toward compression. This effect is more pronounced for aluminum substrate, where the thermal mismatch is larger.

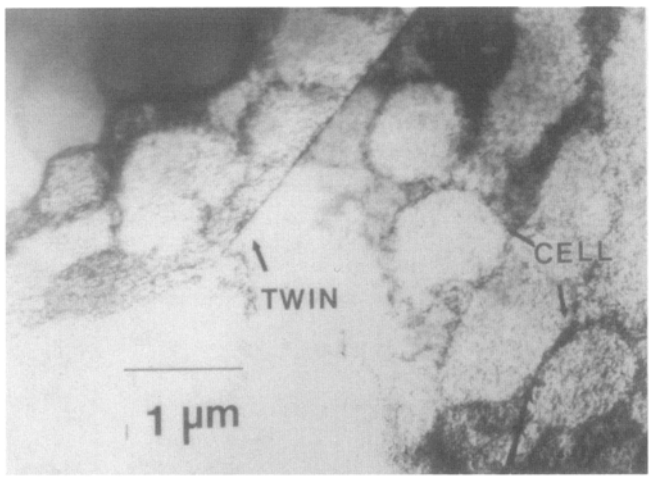

Fig. 3 Transmission electron micrograph of the vacuum plasma spraying nickel coating. Dislocation cells show polygonization, a precursor to recrystallization (Ref 39).

Figures 5 and 6 illustrate the influence of coating thickness. Figure 5 shows the surface stresses in individual specimens of given thickness. The stress in the thinnest layer is relatively high, approximately 100 MPa; for higher thicknesses it retains a roughly constant value, about 40 MPa. Tensile stress in the surface layer is a result of quenching of the impinging splat; as it cools down, its shrinkage is restricted by adherence to the substrate and the splat is brought into tension (Ref 40).

The difference in stress between the first and subsequent coating layers might be explained by a difference in adhesion strength between the first and subsequent layers. The first layer is deposited on a bulk material substrate, whereas later layers arrive on previously deposited coating whose strength can be reduced by pores and imperfect interlamellar contact. This is probably the limiting factor that keeps the maximum stress at approximately constant value (Ref 36).

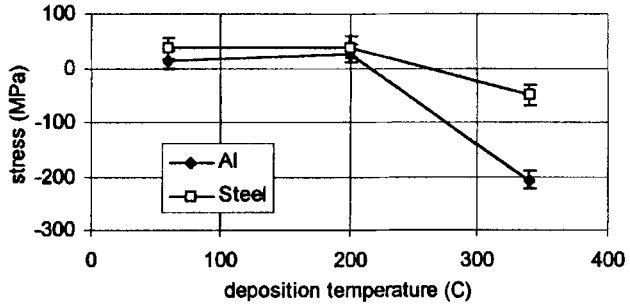

Fig. 4 Residual stresses in thin molybdenum coatings on steel and aluminum, deposited at different temperatures

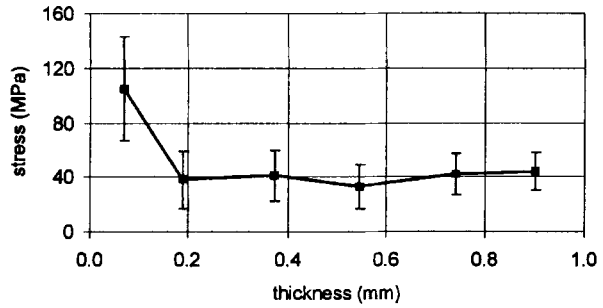

Fig. 5 Surface stress in molybdenum coatings as a function of coating thickness

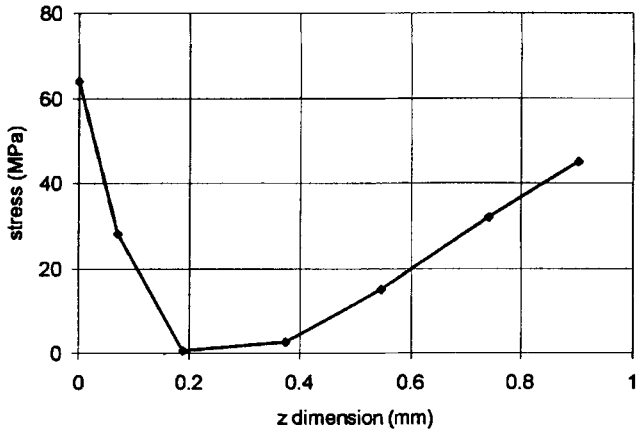

Fig. 6 Stress profile in the 0.9 mm thick molybdenum deposit, calculated from the measured data in Fig. 5

Figure 6 shows the stress profile in the full thickness coating (0.9 mm) calculated from the previous data. The deposition process was approximated by using six layers, each of which was treated as deposited at once. This simplification only determines how finely or coarsely the actual stress profile will be traced, but does not induce any overall bias, as shown by Tsui and Clyne (Ref 41). The stress distribution after each step was simulated using the Multitherm program (Ref 8) so that the surface stress matched the measured value; the stress change in the inner layers due to deposition of a new layer was calculated from force and moment balance (Ref 11). The tensile stress in the newly deposited layer puts the underlying materials into compression, and the resulting moment is accommodated by bending of the substrate. The substrate compliance is the main factor giving rise to the nonlinear stress profile (Ref 42).

5. Conclusions

The x-ray diffraction method of macroscopic stress measurement was applied to selected metallic and ceramic coatings. The capabilities and limitations of the method were examined and discussed. The assumptions underlying the use of common "$\sin^2\psi$" method were scrutinized. The results show that most of the assumptions are applicable; however, the unique structure of the coatings makes its use somewhat complicated, and the simple routines used on bulk materials should not be mechanically reproduced.

Comparison of three different methods for residual stress measurement showed qualitative agreement. Differences in residual stress levels in same material coatings produced under different conditions illustrate the capability of processing parameter selection to modify the stress to a desired state.

Acknowledgment

This research was supported in part by the MRSEC program of the National Science Foundation under award number DMR 9632570 and by the NSF International Program INT 9317415. Jirí Dubsky's research work was sponsored by Grant Agency of the Czech Republic (grant No. GA CR 106/97/0775).

References

1. T.W. Clyne and S.C. Gill, Residual Stresses in Thermally Sprayed Coatings and Their Effect on Interfacial Adhesion—A Review of Recent Work, *J. Therm. Spray Technol.*, Vol 5 (No. 4), 1996, p 401-418
2. V. Dolhof, J. Musil, M. Cepera, and J. Zeman, Stress Analysis of Thermal Sprayed Coatings Using a Semi-Destructive Hole-Drilling Strain Gauge Method, *Thermal Spray Science and Technology*, C.C. Berndt and S. Sampath, Ed., ASM International, 1995, p 445-449
3. D.J. Greving, E.F. Rybicki, and J.R. Shadley, Effects of Coating Thickness and Residual Stresses on Bond Strength of C633-79 Thermal Spray Coating Test Specimens, *Thermal Spray Industrial Applications*, C.C. Berndt and S. Sampath, Ed., ASM International, 1994, p 647-653
4. E.F. Rybicki, J.R. Shadley, Y. Xiong, and D.J. Greving, In Situ Evaluation of Young's Modulus and Poisson's Ratio Using a Cantilever Beam

Specimen, *Thermal Spray Science and Technology,* C.C. Berndt and S. Sampath, Ed., ASM International, 1995, p 409-414
5. X. Provot, H. Burlet, M. Vardavoulias, M. Jeandin, C. Richard, J. Lu, and D. Manesse, Comparative Studies of Microstructures, Residual Stress Distributions and Wear Properties for HVOF and APS WC-Co Coatings on Ti6Al4V, *Thermal Spray: Research, Design and Applications,* C.C. Berndt and T.F. Bernecki, Ed., ASM International, 1993, p 159-166
6. S.C. Gill and T.W. Clyne, Stress Distributions and Material Response in Thermal Spraying of Metallic and Ceramic Deposits, *Metall. Trans. B,* Vol 21 (No. 2), 1990, p 377-385
7. O.C. Brandt, Measuring of Residual Stresses in Thermal Sprayed Coatings, *Thermal Spray Science and Technology,* C.C. Berndt and S. Sampath, Ed., ASM International, 1995, p 451-455
8. M. Finot, S. Suresh, C. Bull, and S. Sampath, Curvature Changes during Thermal Cycling of a Compositionally Graded Ni-Al2O3 Multi-Layered Material, *Mat. Sci. Eng. A,* Vol 205, 1996, p 59-71
9. P. Scardi, M. Leoni, and L. Bertamini, Influence of Phase Stability on the Residual Stress in Partially Stabilized Zirconia TBC Produced by Plasma Spray, *Surf. Coat. Technol.,* Vol 76 (No. 1-3), 1995, p 106-112
10. S. Kuroda and T.W. Clyne, The Quenching Stress in Thermally Sprayed Coatings, *Thin Solid Films,* Vol 200 (No. 1), 1991, p 49-66
11. O. Kesler, M. Finot, S. Suresh, and S. Sampath, Determination of Processing-Induced Stresses and Properties of Layered and Graded Coatings: Experimental Method and Results for Plasma-Sprayed Ni-Al2O3, *Acta Mater.,* Vol 45 (No. 8), 1997, p 3123-3134
12. R. Hamacha, B. Dionnet, A. Grimaud, and F. Nardou, Residual Stress Evolution during the Thermal Cycling of Plasma-Sprayed Zirconia Coatings, *Surf. Coat. Technol.,* Vol. 80 (No. 3), 1996, p 295-302
13. I. Kraus and V.V. Trofimov, *X-Ray Stress Measurement,* Academia, Prague, 1988 (in Czech)
14. H.P. Klug and L.E. Alexander, *X-Ray Diffraction Procedures for Polycrystalline and Amorphous Materials,* John Wiley & Sons, New York, 1974
15. H. Zantopulos and C.F. Jatczak, Systematic Errors in X-Ray Diffractometer Stress Measurements Due to Specimen Geometry and Beam Divergence, *Adv. X-Ray Anal.,* Vol 14, 1971, p 91-103
16. S. Fischer, H.R. Maier, and E. Houtman, High Resolution X-Ray Residual Stress Analysis Based on Tetragonal Zirconia, *Proc. Eur. Conf. on Residual Stresses,* Frankfurt a. M., Germany, 1992, p 361-367
17. S. Sampath and H. Herman, Rapid Solidification and Microstructure Development during Plasma Spray Deposition, *J. Thermal Spray Tech.,* Vol 5 (No. 4), 1996, p 445-456
18. S. Leigh, "Stereological Investigation on Structure/Property Relationships of Plasma Sprayed Deposits," Ph.D. thesis, State University of New York, Stony Brook, 1996
19. R. McPherson, A Review of Microstructure and Properties of Plasma Sprayed Ceramic Coatings, *Surf. Coat. Tech.,* Vol 39-40 (No. 1-3), 1989, p 173-181
20. J. Ilavsky, A.J. Allen, G.G. Long, H. Herman, and C.C. Berndt, Characterization of the Closed Porosity in Plasma-Sprayed Alumina, *J. Mater. Sci.,* Vol 32 (No. 13), 1997, p 3407-3410
21. I. Iordanova, K.S. Forcey, B. Gergov, and V. Bojinov, Characterization of Flame-Sprayed and Plasma-Sprayed Pure Metallic and Alloyed Coatings, *Surf. Coat. Technol.,* Vol 72 (No. 1-2), 1995, p 23-29
22. I. Iordanova, D. Neov, K.S. Forcey, E. Abadjieva, and R. Bezdushnyi, An Analysis of the Influence of Crystallographic Texture on Residual Stress Estimation for Metallic Films and Coatings, *Mater. Sci. Forum,* Vol 228-231, 1996, p 311-316
23. R.H. Marion and J.B. Cohen, Anomalies in Measurement of Residual Stress by X-Ray Diffraction, *Adv. X-Ray Analysis,* Vol 18, 1976, p 466-501
24. I.C. Noyan and J.B. Cohen, *Residual Stress—Measurement by Diffraction and Interpretation,* Springer-Verlag, New York, 1987
25. M. Ceretti, H. Michaud, M. Perrin, and A. Lodini, Residual Stress Measurement in a Plasma Semi-Transferred Arc (PTA) Coating by Neutron and X-ray Diffraction, *Exp. Tech.,* Vol 19 (No. 3), 1995, p 17-21
26. H. Dolle and J.B. Cohen, Residual Stresses in Ground Steels, *Metall. Trans. A,* Vol 11A (No. 1), 1980, p 159-164
27. V.M. Hauk, R.W.M. Oudelhoven, and G.J.H. Vaessen, The State of Residual Stress in the Near Surface Region of Homogeneous and Heterogeneous Materials after Grinding, *Metall. Trans. A,* Vol 13 (No. 7), 1982, p 1239-1244
28. I.C. Noyan, Effect of Gradients in Multiaxial Stress States on Residual Stress Measurements with X-Rays, *Metall. Trans. A,* Vol 14 (No. 2), 1983, p 249-258
29. P. Gondi, G. Mattogno, R. Montanari, and A. Sili, On the Origin of the Residual Stress psi Splitting, *Z. Metallkd.,* Vol 81 (No. 8,) 1990, p 570-575
30. H. Furuichi, Unusual Arrangement of the Inclinations of Lattice Planes and psi Splitting, *Wear,* Vol 113 (No. 3), 1986, p 323-329
31. M.M. Gola and P. Coppa, Possible Experimental X-Ray Diffractometry Evidence of Couple-Stresses, *J. Appl. Mech.,* Vol 55 (No. 3), 1988, p 539-544
32. I. Kraus and G. Gosmanová, X-Ray Diffraction Analysis of Macrostresses in Surface Layers of Metallic Materials, *Met. Mater.,* Vol 28 (No. 3), 1990, p 75-79
33. S. Tobe, H. Misawa, K. Akita, and Y. Kon, Macro- and Microstress in Plasma Sprayed Coatings and Its Stress vs. Strain Behavior, *Thermal Spray Industrial Applications,* C.C. Berndt and S. Sampath, Ed, ASM International, 1994, p 693-697
34. S.C. Gill, "Residual Stresses in Plasma Sprayed Deposits," Ph.D. thesis, University of Cambridge, Cambridge, UK, 1991
35. J. Dubsky, B. Kolman, P. Ctibor, and F. Kroupa, Structure and Residual Stresses in Thermally Sprayed Steel Coatings, *Fifth Int. Symp. on Functionally Graded Materials,* Dresden, Germany, 1998
36. S. Kuroda, T. Fukushima, and S. Kitahara, Significance of the Quenching Stress in the Cohesion and Adhesion of Thermally Sprayed Coatings, *Thermal Spray: International Advances in Coatings Technology,* C.C. Berndt, Ed., ASM International, 1992, p 903-909
37. M. Levit, I. Grimberg, and B. Z. Weiss, Residual Stress in Ceramic Plasma-Sprayed Thermal Barrier Coatings: Measurement and Calculation, *Mater. Sci. Eng. A,* Vol. 206, 1996, p 30-38
38. P. Scardi, M. Leoni, and L. Bertamini, Residual Stresses in Plasma Sprayed Partially Stabilised Zirconia TBCs: Influence of the Deposition Temperature, *Thin Solid Films,* Vol 278 (No. 1-2), 1996, p 96-103
39. S. Sampath, "Rapid Solidification during Plasma Spraying," Ph.D. thesis, State University of New York, Stony Brook, 1989
40. J. Matejicek, S. Sampath, and J. Dubsky, Residual Stress Measurement in Plasma Sprayed Coatings by X-Ray Diffraction, *Thermal Spray: A United Forum for Scientific and Technological Advances,* C.C. Berndt, Ed., ASM International, 1997, p 855-860
41. Y.C. Tsui and T.W. Clyne, An Analytical Model for Predicting Residual Stresses in Progressively Deposited Coatings, *Thin Solid Films,* Vol 306 (No. 1), 1997, p 23-61
42. F. Kroupa, Quenching Residual Stresses in Continuously Thermal Sprayed Coatings and Plates, *Acta Tech. CSAV,* Vol 42 (No. 5), 1997, p 591-612